

ANALYZING TIME SERIES OF SATELLITE IMAGERY USING TEMPORAL MAP ALGEBRA

Jeremy Mennis

Department of Geography
University of Colorado
Boulder, CO 80309
jeremy@colorado.edu

Roland Viger

Department of Geography
University of Colorado
Boulder, CO 80309
and
U.S. Geological Survey
MS 412 Box 25046 DFC
Denver, CO, 80225
rviger@usgs.gov

ABSTRACT

This paper presents the application of a set of spatio-temporal satellite image analysis functions based on temporal map algebra. The temporal map algebra functions treat time series of imagery as three-dimensional data sets where two dimensions encode planimetric position on the earth's surface and the third dimension encodes time. Whereas the conventional local, focal, and zonal map algebra functions take as input one or more grids and output a grid (or, in the case of zonal functions, a table), temporal map algebra functions take one or more three-dimensional data 'cubes' as input and output a data 'cube' (or, in the case of temporal zonal functions, a table). As a demonstration of the utility of temporal map algebra for time series satellite image analysis, we investigate the impact of El Niño/Southern Oscillation (ENSO) on the 1982-1993 monthly time series Advanced Very High Resolution Radiometer (AVHRR) Normalized Difference Vegetation Index (NDVI) signal in southern Africa. Results suggest that vegetation intensity is suppressed, and its spatial and temporal variability enhanced, during ENSO warm and cold phase months, particularly over forest, woodland, and wooded grassland. These effects are generally diminished by the following growing season, particularly following an ENSO cold phase. For shrubland, vegetation intensity tends to increase during the growing season following an ENSO cold phase.

INTRODUCTION

Homogeneous time series of satellite imagery are now becoming available due to the establishment and maintenance of long-term earth observing programs. These time-series data sets provide a rich source of information on the dynamic nature of earth surface processes, and have been used for monitoring land cover change, phenology, and vegetation-climate dynamics (Anyamba and Eastman, 1996; Mennis, 2001; Myneni et al., 1998). While a number of statistical techniques have been used for analyzing time series of remotely sensed imagery, such as principle components analysis and spectral analysis (e.g. Eastman and Fulk, 1993; Jakubauskus et al., 2001), a standardized and widely available set of tools for manipulating and analyzing time series of satellite imagery has yet to be developed.

This paper presents the application of a set of spatio-temporal satellite image analysis functions based on temporal map algebra. These functions are temporal extensions to the conventional map algebra found in most geographic information systems (GIS) software packages that support raster data handling. The temporal map algebra functions treat time series of imagery as three-dimensional data sets where two dimensions encode planimetric position on the earth's surface and the third dimension encodes time. Thus, time series of satellite imagery may be manipulated according to well-established and standardized raster processing techniques. As a demonstration of the utility of

temporal map algebra for time series image analysis, we investigate the impact of El Niño/Southern Oscillation (ENSO) on the 1982-1993 monthly time series Advanced Very High Resolution Radiometer (AVHRR) Normalized Difference Vegetation Index (NDVI) signal in southern Africa.

TEMPORAL MAP ALGEBRA

Conventional Map Algebra

Map algebra describes a set of raster processing functions that are typically classified into local, focal, and zonal types (Tomlin, 1990). These functions typically take one or more raster grids as input data layers and generate a separate grid as an output data layer. Local functions compute the value of each individual grid cell in the output grid as a function of the values contained in the analogous grid cell position in the set of input grids. For example, a LOCALMEAN function applied to two input grids will produce an output grid in which each grid cell's value is equal to the mean of the analogous grid cell position values in the two input grids. Note that while the statistical operator 'mean' is discussed here, each of the function types may be applied using a variety of mathematical and statistical operators, such as addition, multiplication, and variance.

Focal functions compute the value of each grid cell in the output grid as a function of the neighborhood surrounding the analogous grid cell position in an input grid. For example, a FOCALMEAN function applied to an input grid will generate an output grid in which each grid cell's value is equal to the mean of all the grid cell values contained within the neighborhood of the analogous grid cell position in the input grid. Note that the neighborhood around a given grid cell position can be a simple 3x3 cell window, a larger, rectangular window, or can take the form of a circular, wedge, or doughnut shape. Zonal functions take as input a value grid and a zone grid and output a table. The table reports a summary of the grid cell values contained in the value grid for each zone specified in the zone grid. For instance, a ZONALMEAN function applied to an elevation grid (the value grid) and a vegetation type grid (the zone grid) will produce a table reporting the mean elevation for each vegetation type.

Extending Map Algebra for Temporal Analysis

While previous researchers have developed temporal map algebra-like algorithms (Mennis and Peuquet, 2003), these implementations have been domain-specific and not generalizable to other data sets. We have developed a set of generic temporal map algebra functions that extend the conventional local, focal, and zonal functions to three dimensions – two spatial dimensions plus a temporal dimension. These temporal map algebra functions may be applied to a variety of spatio-temporal analysis contexts, including the analysis of times series of satellite imagery. Whereas the conventional map algebra functions take as input one or more grids and output a grid (or, in the case of zonal functions, a table), temporal map algebra functions take one or more three-dimensional data 'cubes' as input and output a data 'cube' (or, in the case of temporal zonal functions, a table). The data structure for encoding these data cubes and the temporal map algebra functions themselves were implemented in the interactive data language (IDL) (Research Systems, Inc.).

Temporal local map algebra functions are similar to conventional local map algebra functions except the output data set is a three-dimensional cube instead of a grid, and the value of each cube element (analogous to an individual grid cell, but indicating both spatial and temporal position) is derived from the analogous cube element position in the input cubes. Likewise, temporal focal map algebra functions generate an output cube in which the value of each cube element is derived from the neighborhood surrounding the analogous cube element position in the input cube. However, whereas in conventional focal map algebra functions the neighborhood is defined as a spatial region, in temporal map algebra the neighborhood may be defined as a spatial window, temporal extent, or spatio-temporal cube. Temporal zonal map algebra functions output a table that summarizes the cube element values contained in a value cube that fall within zones defined by a zone cube. As with temporal focal map algebra functions, zones for temporal zonal map algebra functions may be spatial, temporal, or spatio-temporal in nature.

ANALYSIS OF ENSO-VEGETATION DYNAMICS IN SOUTHERN AFRICA



Figure 1. The study region.

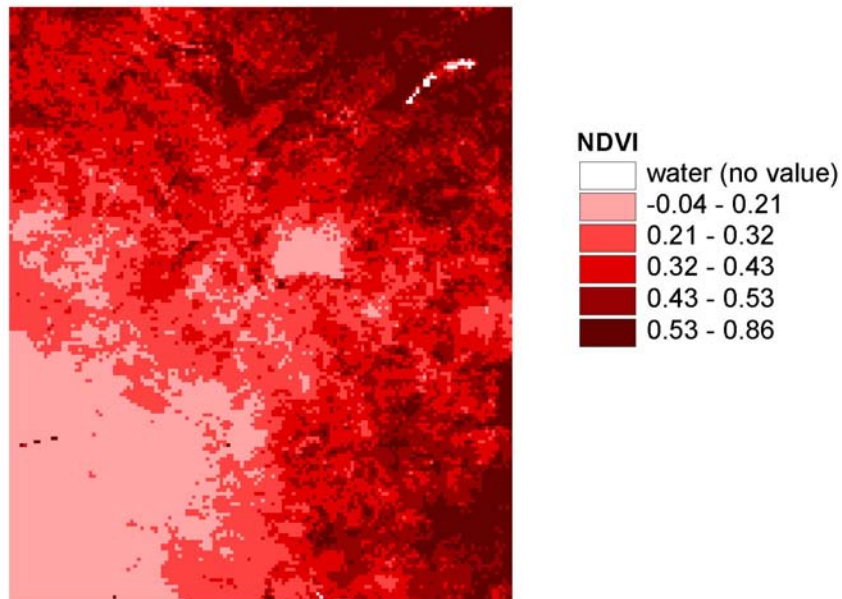


Figure 2. Study region NDVI for January 1982.

Data

The temporal map algebra functions were used to analyze the relationship of ENSO with vegetation dynamics over different land covers in an approximately 1.5 million km² area of southern Africa (Figure 1). Previous research has indicated the vegetation intensity of this region to be sensitive to ENSO dynamics (Anyamba and Eastman,

1996). Monthly 1982-1993 AVHRR NDVI data covering the study region were acquired from the Pathfinder AVHRR Land (PAL) program via the Distributed Active Archive Center at NASA Goddard Space Flight Center (Figure 2). These 8 km resolution data are generated from ten day composite 1 km resolution imagery in which the maximum pixel value over a ten day period is retained and to which corrections for atmospheric attenuation have been applied (Teng, 1999). Land cover data at an 8 km resolution were acquired from the Global Land Cover Facility at the University of Maryland (Figure 3). These data were generated through the application of high resolution satellite imagery to identify appropriate training pixels from 1 km resolution PAL program data (DeFries et al. 1998). A series of metrics derived from these data were then input into a decision tree classifier to yield the land cover data set (Hansen et al. 2000). The study region is dominated by woodland, wooded grassland, and shrubland, with smaller areas of cropland and forest.

Data indicating the 1982-1993 monthly ENSO phase (warm [El Niño], cold [La Niña], or neutral) were acquired from the National Oceanic and Atmospheric Administration (NOAA)-Cooperative Institute for Research in Environmental Sciences' (CIRES) Climate Diagnostics Center. These data were generated by identifying those months that exceed the twentieth percentile in the anomaly from the long term five month running mean for both the Southern Oscillation Index (SOI) and the sea surface temperature (SST) for Niño 3.4, an ENSO-sensitive region of the equatorial Pacific Ocean (Smith and Sardeshmukh, 2000). Warm phases are recorded for select months during 1982-1983, 1987, 1991-1992, and 1993, while a cold phase is recorded for three months in 1988.

Methods and Results

In order to investigate the broad impact of ENSO on the vegetation of the study region, the mean NDVI for each ENSO phase over the entire region was calculated using a temporal map algebra ZONALMEAN function in which the zone cube described the ENSO phases and the value cube contained the NDVI data. The result of this function reported the mean NDVI for ENSO warm, cold, and neutral phases to be 0.28, 0.26, and 0.32, respectively. The neutral phase clearly tends to have the highest NDVI values over the region. Another temporal map algebra ZONALMEAN function was used to calculate the mean NDVI for each land cover class. Results are presented in Table 1. Forest areas tend to have the highest NDVI values, followed by woodland, grassland and cropland, and then shrubland.

A temporal map algebra LOCALSUM function was used to combine the ENSO phase and land cover zone cubes to produce a new zone cube where each zone encoded a unique ENSO phase/land cover combination. The mean NDVI for each land cover for each ENSO phase was then calculated using a temporal map algebra ZONALMEAN function where the newly generated ENSO phase/land cover data served as the zone cube and the NDVI data served as the value cube. Results are reported in Table 2. All land covers have higher mean NDVI values during an ENSO neutral phase as compared to warm or cold phases. Forest, woodland, and wooded grassland have markedly lower ENSO cold phase mean NDVI values as compared with their warm phase values. Shrubland, grassland, and cropland have similar mean NDVI values for ENSO warm and cold phases.

The spatial, temporal, and spatio-temporal variability of NDVI may also be of interest. To investigate the nature of NDVI variation over different land covers and during different ENSO phases, a temporal map algebra FOCALVARIANCE function was used to calculate NDVI variance. Variance was calculated using both a

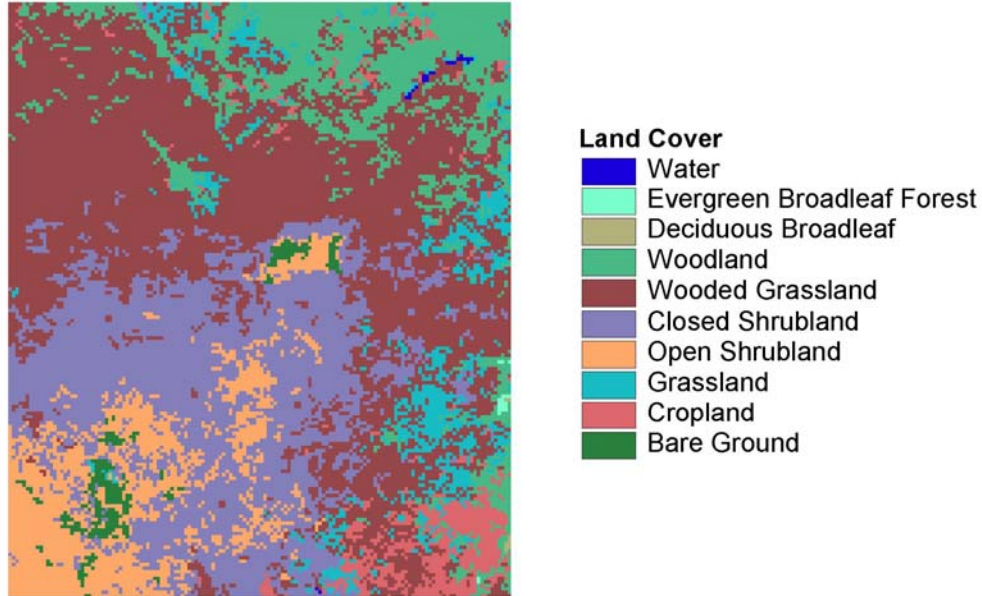


Figure 3. Study region land cover.

Table 1. Mean 1982-1993 NDVI by Land Cover

Land Cover	NDVI
Evergreen Broadleaf Forest	0.61
Deciduous Broadleaf Forest	0.56
Woodland	0.43
Woodland Grassland	0.34
Closed Shrubland	0.23
Open Shrubland	0.18
Grassland	0.37
Cropland	0.37
Bare Ground	0.14

Table 2. Mean 1982-1993 NDVI by Land Cover and ENSO Phase

Land Cover	Warm Phase	Neutral Phase	Cold Phase
Evergreen Broadleaf Forest	0.60	0.61	0.54
Deciduous Broadleaf Forest	0.53	0.56	0.51
Woodland	0.40	0.45	0.32
Wooded Grassland	0.31	0.35	0.27
Closed Shrubland	0.21	0.24	0.22
Open Shrubland	0.17	0.18	0.17
Grassland	0.33	0.38	0.32
Cropland	0.33	0.38	0.34
Bare Ground	0.14	0.15	0.14

Table 3. Mean 1982-1993 Spatial, Temporal, and Spatio-Temporal NDVI Variance by Land Cover and ENSO Phase

Neighborhood	Land Cover 2	Warm Phase	Neutral Phase	Cold Phase
3x3x1 Spatial Variance	Evergreen Broadleaf Forest	0.0116	0.0113	0.0134
	Deciduous Broadleaf Forest	0.0034	0.0038	0.0083
	Woodland	0.0022	0.0022	0.0032
	Wooded Grassland	0.0014	0.0015	0.0019
	Closed Shrubland	0.0010	0.0010	0.0010
	Open Shrubland	0.0007	0.0008	0.0006
	Grassland	0.0018	0.0019	0.0024
	Cropland	0.0016	0.0016	0.0024
	Bare Ground	0.0012	0.0014	0.0010
1x1x3 Temporal Variance	Evergreen Broadleaf Forest	0.0042	0.0048	0.0103
	Deciduous Broadleaf Forest	0.0040	0.0038	0.0068
	Woodland	0.0059	0.0072	0.0077
	Wooded Grassland	0.0040	0.0051	0.0054
	Closed Shrubland	0.0024	0.0028	0.0028
	Open Shrubland	0.0012	0.0016	0.0011
	Grassland	0.0041	0.0050	0.0063
	Cropland	0.0057	0.0063	0.0091
	Bare Ground	0.0013	0.0015	0.0007

3x3x1 element spatial-only focal neighborhood and a 1x1x3 element temporal-only focal neighborhood. A temporal map algebra ZONALMEAN function was then used to calculate the mean NDVI variance for each ENSO phase/land cover class using each of the two focal neighborhood types. Results are reported in Table 3. Generally, the spatial variation of NDVI tends to be higher during an ENSO cold phase as compared to warm and neutral phases. The exceptions are for shrubland and bare ground, for which there is no discernable difference in spatial variation among ENSO phases. Temporal variation in NDVI tends to be greatest during an ENSO cold phase, and greater during a warm phase as compared with a neutral phase. Again, the exception is for shrubland, for which there is no discernable pattern.

These results are broadly consistent with established southern African climatological responses to ENSO warm phases, which are typically associated with drought and thus a decrease in vegetation intensity. However, these results run counter to other studies that have found an increase in vegetation intensity over southern Africa during

ENSO cold phase events (Anyamba and Eastman, 1996), due to associated wetter weather (Nicholson and Salato, 2000). This discrepancy may be due to the suppression of NDVI values during ENSO cold phases from increases in soil moisture or through flooding. It should also be noted that only one ENSO cold phase occurred during the 1982-1993 study period, which may not be representative of most ENSO cold phases. In addition, a temporal trend in the NDVI signal may be present due to sensor calibration and orbital drift that has not been accounted for in this research.

It has also been suggested that the effects of an ENSO cold phase event in southern Africa are greatest in the early months of the year following the observed ENSO event, when vegetation intensity annually peaks. As a means to investigate this, the mean NDVI for each land cover was recalculated for the January-April period following each ENSO warm, cold, and neutral phase. Results are presented in Table 4. Interestingly, Table 4 generally shows less difference among ENSO warm, cold, and neutral phases among most land cover classes as compared to Table 3. Of particular note are the results for shrubland, for which Table 4 shows a higher mean NDVI value for ENSO cold phases as compared to warm and neutral phases.

Table 4. Mean 1982-1993 NDVI by Land Cover and the January-April Period Following each ENSO Phase

Land Cover	Warm Phase	Neutral Phase	Cold Phase
Evergreen Broadleaf Forest	0.65	0.66	0.61
Deciduous Broadleaf Forest	0.60	0.64	0.65
Woodland	0.54	0.56	0.54
Wooded Grassland	0.43	0.42	0.45
Closed Shrubland	0.29	0.28	0.36
Open Shrubland	0.21	0.20	0.27
Grassland	0.44	0.46	0.46
Cropland	0.46	0.50	0.51
Bare Ground	0.17	0.15	0.23

CONCLUSION

This research has demonstrated the application of temporal map algebra to the analysis of time series of satellite imagery through an analysis of ENSO-vegetation dynamics over different land covers in southern Africa. This analysis clearly shows that the effect of ENSO on vegetation intensity in southern Africa varies over different land covers. Note that this analysis could easily be extended in a number of ways, while still using the basic temporal map algebra functions described here. For instance, one could investigate the time lag in the impact of ENSO on vegetation intensity. A more thorough analysis of the spatial, temporal, and spatio-temporal variation in NDVI could be accomplished by simply experimenting with different neighborhood settings of the temporal map algebra FOCALVARIANCE function. In future research we plan to continue the development of the temporal map algebra functions presented here for a more extensive spatio-temporal analysis of NDVI over Africa. We also intend to demonstrate how temporal map algebra may be applied to a variety of other time series imagery data sets.

ACKNOWLEDGMENTS

The authors would like to thank Dana Tomlin for conversations inspiring this research and Jun Wei Liu for data preprocessing. Thanks also to NASA Goddard Space Flight Center and the University of Maryland for providing data. This research was supported by a NASA New Investigator Program grant (NAG5-12598).

REFERENCES

- Anyamba, A., and J. R. Eastman (1996). Interannual variability of NDVI over Africa and its relation to El Niño / Southern Oscillation. *International Journal of Remote Sensing*, 17(13):2533-2548.
- DeFries, R., M. Hansen, J. R. G. Townshend, and R. Sohlberg, (1998). Global land cover classifications at 8 km spatial resolution: The use of training data derived from Landsat imagery in decision tree classifiers. *International Journal of Remote Sensing*, 19:3141-3168.
- Eastman, J. R. and M. Fulk (1993). Long sequence time series evaluation using standardized principal components. *Photogrammetric Engineering and Remote Sensing*, 59(8):1307-1312.
- Hansen, M., R. DeFries, J. R. G. Townshend, and R. Sohlberg (2000). Global land cover classification at 1km resolution using a decision tree classifier. *International Journal of Remote Sensing*, 21:1331-1365.
- Jakubauskas, M.E., D.R. Legates, and J. Kastens (2001). Harmonic analysis of time-series AVHRR NDVI data. *Photogrammetric Engineering and Remote Sensing*, 67(4):461-470.
- Mennis, J. (2001). Exploring relationships between ENSO and vegetation vigour in the south-east USA using AVHRR data. *International Journal of Remote Sensing*, 22:3077-3092.
- Mennis, J. and D. Peuquet (2003). The role of knowledge representation in geographic knowledge discovery: a case study. *Transactions in GIS*, 7(3):371-391.
- Myneni, R. B., C. J. Tucker, G. Asrar, and C. D. Keeling (1998). Interannual variations in satellite-sensed vegetation index data from 1981 to 1991. *Journal of Geophysical Research* 103(D6):6145-6160
- Nicholson, S. E. and J. C. Selato (2000). The influence of La Niña on African rainfall. *International Journal of Climatology*, 20:1761-1776.
- Smith, C.A. and P. Sardeshmukh (2000). The effect of ENSO on the intraseasonal variance of surface temperature in winter. *International Journal of Climatology*, 20:1543-1557.
- Teng, W. (1999). NDVI Data from AVHRR Land Pathfinder. WWW Document: http://daac.gsfc.nasa.gov/CAMPAIGN_DOCS/FTP_SITE/INT_DIS/readmes/pal.html, last accessed February 13, 2004.
- Tomlin, C. D. (1990). *Geographic Information Systems and Cartographic Modeling*. Prentice Hall, Englewood Cliffs, New Jersey.